ACS APPLIED NANO MATERIALS

www.acsanm.org

Article

Upconverting Nanoparticles and Cu(I) Complex-Based Platform for Oxygen Sensing, Thermometry, and Emission Color Tuning

Marylyn Setsuko Arai,*,# Leandro Piaggi Ravaro,# Gabriel Brambilla, Lauro June Queiroz Maia, Mohammad Reza Dousti, and Andrea Simone Stucchi de Camargo*

Cite This: *ACS Appl. Nano Mater.* 2025, 8, 854−862

Read Online

ACCESS | Metrics & More | Article Recommendations | Supporting Information

ABSTRACT: Multifunctional nanoplatforms combine different material properties to meet a wide range of applications, allowing highly customizable systems. In this rapidly advancing research field, we introduce a multifunctional nanomaterial based on the synergy between Tm^{3+}-doped upconverting nanoparticles (UCNPs) and a Cu(I) complex (CuCom). This material is designed for oxygen sensing, optical thermometry, and emission color tuning. In various concentrations, the CuCom complex was electrostatically integrated into a mesoporous silica shell surrounding the core UCNPs (UCNP@mSiO_2). The optimized system, UCNP@mSiO_2@CuCom-10, was evaluated for different applications. Due to the spectral overlap between the CuCom absorption and the nanoparticles emission, excitation at 980 nm allows most of the UV-blue emission output from the UCNPs to be transferred to the CuCom via luminescent resonance energy transfer (LRET), producing red emission from the molecule. The remaining Tm^{3+} emission enables optical thermometry, while CuCom's sensitivity to molecular oxygen supports its application in gas sensing. In upconversion mode, the nanoplatform achieved a Stern−Volmer constant for O_2 sensing of 1.64 and demonstrated thermometric relative sensitivities of 0.9% and 1% K^{-1} at room temperature, with a linear response from 193 to 373 K. Additionally, the emission color of UCNP@mSiO_2@CuCom-10 can be tuned from blue to white and yellow, by varying the excitation and temperature, adding further functionality to the system. This multifunctional platform suggests promising applications in biology, medicine, and environmental monitoring.

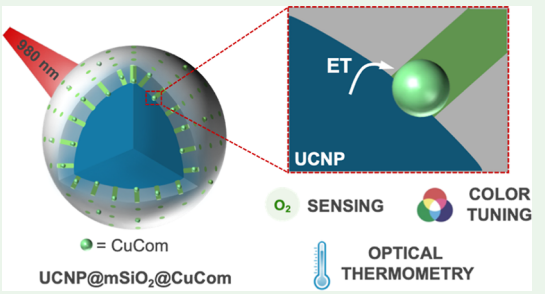

KEYWORDS: *multifunctional nanomaterial, O_2 sensing, upconversion, luminescence resonance energy transfer (LRET), optical thermometry, mesoporous silica shell*

INTRODUCTION

Multifunctional nanoplatforms are attracting increasing attention given their ability to combine electronic, optical, magnetic, and catalytic properties. These platforms are based on the association of functional materials, so their synergetic properties differ from those of the individual components and are designed to meet diverse application requirements.[1] The high surface area to volume ratio, quantum effects, tunable properties, and enhanced performance of nanomaterials have paved the way for the development of advanced multifunctional nanoscopic platforms.[2,3]

In this scenario, luminescent nanomaterials have been widely explored and, among them, upconverting nanoparticles (UCNPs) stand out due to their unique properties, such as anti-Stokes emission and excitation wavelengths within the biological window. UCNPs are nanocrystals capable of converting low-energy excitation into higher-energy emission photons through multiphoton absorption processes.[4,5] These particles present narrow absorption/emission bands, long luminescence lifetimes (μs), and large Stokes shifts. Their use has overcome several drawbacks associated with conventional phosphors, such as photodegradation, blinking, high toxicity, autofluorescence, and the requirement for biologically harmful UV excitation sources.[6−8] The $NaYF_4$:Yb^{3+},Tm^{3+} nanocrystals are among the most employed UCNPs due to their exceptional luminescent properties, with excitation at 980 nm and emissions in the UV−visible. Recently, these nanoparticles have been applied in optical nanothermometry[9,10] with high spatial resolution and have enabled: (i) the study of temperature distributions in biological nanostructures, cells, and tissues; (ii) noninvasive measurements, which is a crucial feature in biological applications where invasive methods can damage the sample and (iii) real-time monitoring, which is beneficial for dynamic processes.

The prospect of creating a multifunctional nanoplatform by associating the unique properties of UCNPs with low-cost and high-performance materials at the molecular level led to our

Received: November 11, 2024
Revised: December 4, 2024
Accepted: December 6, 2024
Published: December 13, 2024

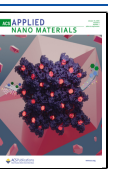

interest in Cu(I) complexes, which have proven to be excellent candidates for applications including lighting (OLEDs),[11] bioimaging,[12] thermometry,[13] vapochromism,[14] and gas sensing.[15,16] Cu(I) complexes exhibit broad visible emissions from blue to red due to metal-to-ligand charge transfer (MLCT) and also present large Stokes shifts.[17,18] The easy manipulation and combination of some Cu(I) complexes with appropriate host matrices allowed the development of remote sensors with very sensitive responses to O_2 presence, which is crucial in various domains.[19,20] These sensors have found applications in biology (monitoring cellular respiration and hypoxia response), medicine (patient monitoring and disease diagnosis), environmental monitoring (pollution and climate change), and in the industrial grounds of safety and quality control.[21−23]

In a previous work, we demonstrated oxygen sensing in both downshifting and upconversion modes, by integrating Tm-UCNPs with CuCom into a polystyrene (PS) host matrix.[24] PS was chosen for its transparency, oxygen permeability, compatibility with embedded materials, and ability to accommodate different concentrations of CuCom. However, the resulting macroscopic hybrid system was unsuitable for nanoscale applications. Taking a step forward in the development, in this work we have combined the nanoparticles and complex by directly adding the molecules to the mesoporous silica shell that coats the UCNP surface (UCNP@$mSiO_2$). The silica shell offers very similar transparency, high oxygen permeability, and host compatibility as the PS matrix, allowing the maintenance of the multifunctionality on nanoscale.

Besides oxygen sensing, the new nanomaterial based on the combination of Tm-UCNP@$mSiO_2$ and Cu(I) complexes, also performs optical thermometry and presents emission color-tuning, allowing for control and customization of light emission upon temperature and excitation wavelength selection, which enhances the system's functionality. Specifically, the nanomaterial is based on highly emissive $NaYF_4$:20% Yb^{3+}, 0.3% Tm^{3+}@$NaYF_4$ UCNPs coated with a mesoporous silica shell and electrostatically combined with the $Cu_2I_2(DPP)-(PPh_3)_2$ complex (CuCom, where DPP = diphenyl-2-pyridyl-phosphine and PPh_3 = triphenylphosphine) to create $NaYF_4$:20% Yb^{3+}, 0.3% Tm^{3+}@$NaYF_4$@$mSiO_2$@CuCom (from now on called UCNP@$mSiO_2$@CuCom). In this system, the complex can be directly activated in the UV range; however, the use of high-energy radiation strongly hinders applications in biological media where excitation in the infrared window is much preferred. Therefore, we explored the fact that CuCom has an absorption band overlapping with the UCNP emission in the UV-blue region. When the system is excited at 980 nm, part of the nanoparticle's emission is transferred to the complex molecules on their surface to activate their corresponding luminescence in the red. The remaining blue emission of the UCNPs is used for optical thermometry, while the CuCom red emission is explored in oxygen sensing. We envision promising applications of the UCNP@$mSiO_2$@CuCom synergistic nanoplatform, both in the medical and biological fields, following cellular respiration and hypoxia response, as well as temperature distributions in bio tissues, and in environmental monitoring for controlling fluctuations in oxygen concentration and temperature, which often occur concomitantly.

EXPERIMENTAL SECTION

Nanoparticles Production. *Synthesis of β-UCNPs ($NaYF_4$:25% Yb^{3+}, 0.3% Tm^{3+}).* UCNPs with hexagonal structure were synthesized following a high-temperature coprecipitation method as previously reported.[35] $LnCl_3$ aqueous solutions [0.747 mL YCl_3 (1 M), 0.25 mL $YbCl_3$ (1 M), and 0.3 mL $TmCl_3$ (0.01 M)] were transferred to a 100 mL three-necked round-bottom flask and heated to evaporate water. The resulting powder was mixed with 6 mL oleic acid (OA) and 15 mL octadecene (ODE), heated to 150 °C for 30 min under nitrogen or argon atmosphere to form a homogeneous solution, and then cooled down to room temperature. Five mL of a methanol solution containing NaOH (0.1 g) and NH_4F (0.148 g) were slowly added into the flask, which led to the formation of solid-state precipitates in the solution. Subsequently, the solution was slowly heated to 110 °C to evaporate methanol, degassed for 10 min, and then heated to 300 °C and maintained for 1 h under an inert atmosphere. After the solution was naturally cooled down, nanocrystals were precipitated with acetone, isolated via centrifugation (6000 rpm, 10 min), and washed once with acetone and twice with ethanol.

UCNPs Coating with a Shell of the Undoped Matrix ($NaYF_4$:Yb/Tm@$NaYF_4$ = Tm-UCNP). The procedure to coat the nanoparticles with an inert matrix shell was similar to the one used for the synthesis of core UCNPs. First, 1 mL of YCl_3 aqueous solution (1 M) was transferred to a 100 mL three-necked round-bottom flask and heated until dried. The resulting powder was mixed with 6 mL OA, and 15 mL ODE and heated to 150 °C for 30 min to form a yellow homogeneous and clear solution. After cooling to room temperature, as-prepared UCNPs (redispersed in 15 mL of cyclohexane) were added to the above solution, and the mixture was heated to 100 °C. After removing cyclohexane, the synthesis proceeded following the same steps as that of $NaYF_4$:Yb, Tm nanoparticles. The final core-shell nanocrystals were washed with acetone one time, with ethanol two times, and dried at room temperature.

UCNPs Coating with a Mesoporous Silica Shell (UCNP@$mSiO_2$). The UCNPs were coated with mesoporous silica following a previously reported two-phase microemulsion procedure with slight modifications.[36] Initially, 19.5 mg of UCNPs were dispersed in 1.95 mL of chloroform and mixed with 15 mL of CTAB solution (0.05 M) under vigorous stirring for about 30 min, which led to a homogeneous oil-in-water microemulsion. Afterwards, the mixture was heated to 90 °C under vigorous stirring to evaporate chloroform and obtain a transparent solution of nanocrystals in water. The solution was then transferred to a 150 mL one-neck round-bottom flask containing 75 mL of basic aqueous solution (pH 10.5). The flask was then placed in an oil bath at 70 °C and stirred gently (about 80 rpm) with a magnetic stirrer. After about 30 min, when the flask content reached the target temperature, 0.75 mL of TEOS in 6 mL of cyclohexane was slowly added to avoid mixing of liquid phases. The heating was turned off, the flask was closed, and the system was kept under gentle stirring (80 rpm) for 24 h. The UCNP@$mSiO_2$ were collected via centrifugation (6000 rpm, 30 min) and washed with DI water (twice) and with ethanol (twice). Finally, the nanoparticles were dispersed in ethanol or kept dry for further characterization.

Synthesis of the $Cu_2I_2(DPP)(PPh_3)_2$ Complex (CuCom). The copper(I) complex was synthesized according to the protocol previously reported by Volz et al.[37] 190 mg of CuI, 131.63 mg of diphenyl-2-pyridyl-phosphine (DPP) and 262.30 mg of triphenyl-phosphine (PPh_3) (1:0.5:1, equivalent) were mixed in 10 mL of dichloromethane under constant stirring, at room temperature, in the dark, and under a stream of nitrogen. After 2 h of stirring, a yellow solution was obtained and then hexane was added to precipitate the molecule. IR (ATR). ν = 490 (s), 504 (s), 516 (s), 618 (vw), 692 (vs), 742 (s), 769 (vw), 850 (vw), 918 (vw), 972 (vw), 997 (vw), 1027 (vw), 1054 (vw), 1070 (vw), 1092 (vw), 1120 (vw), 1156 (vw), 1182 (vw), 1262 (vw), 1285 (vw), 1310 (vw), 1330 (vw), 1432 (m), 1451 (vw), 1478 (w), 1558 (vw), 1573 (vw), 1585 (vw), 3050 cm^{-1} (vw).

CuCom Adsorption to UCNP@$mSiO_2$ (UCNP@$mSiO_2$@CuCom). To prepare the UCNP@$mSiO_2$@CuCom platforms, 15 mg of UCNP@$mSiO_2$ dispersed in 10 mL of methanol were mixed with 5

https://doi.org/10.1021/acsanm.4c06351
ACS Appl. Nano Mater. 2025, 8, 854−862

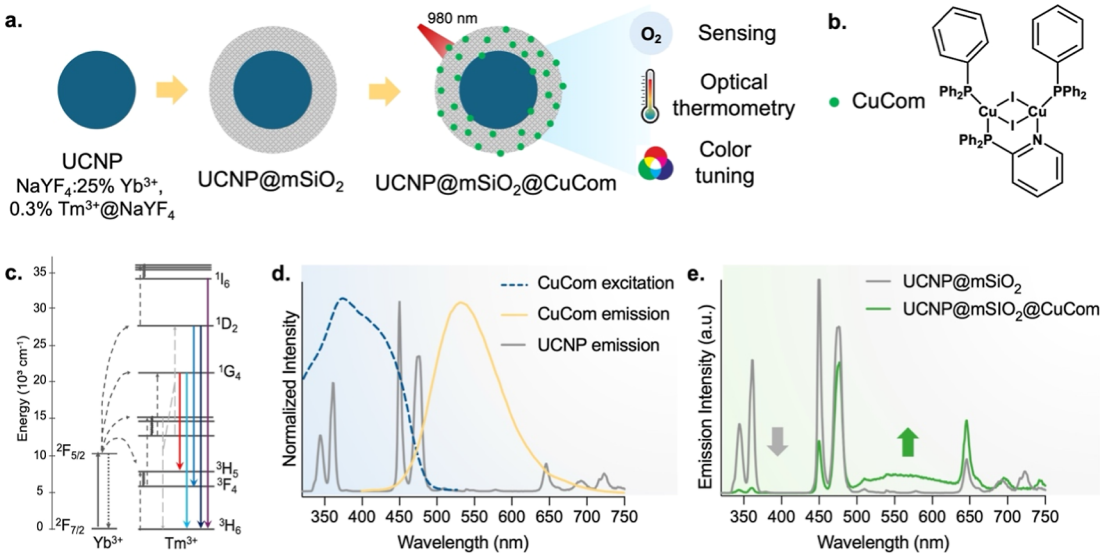

Figure 1. General working principle of the developed nanoplatforms. (a) Schematic representation of the UCNP@$mSiO_2$@CuCom and its oxygen sensing, thermometry, and color tuning properties. (b) Molecular structure of $Cu_2I_2(DPP)(PPh_3)_2$. (c) Partial energy-level diagram of Yb^{3+} and Tm^{3+} and the anti-Stokes processes in Tm-UCNPs: the sensitizer ions Yb^{3+} absorb most of the photons and transfer them to the Tm^{3+} activator ions, which emit UV−visible light. (d) Emission spectra of UCNPs (λ_{exc} = 980 nm) and CuCom (λ_{exc} = 360 nm), and excitation spectrum of CuCom (λ_{em} = 550 nm) showing the overlap between the complex absorption and the nanoparticle UV-blue emission. (e) Comparison between the emission spectra of UCNP@$mSiO_2$ and UCNP@$mSiO_2$@CuCom (λ_{exc} = 980 nm). Upon CuCom's presence, there is a decrease in the UCNP emission in the UV and blue regions and the appearance of the molecule luminescence around 560 nm.

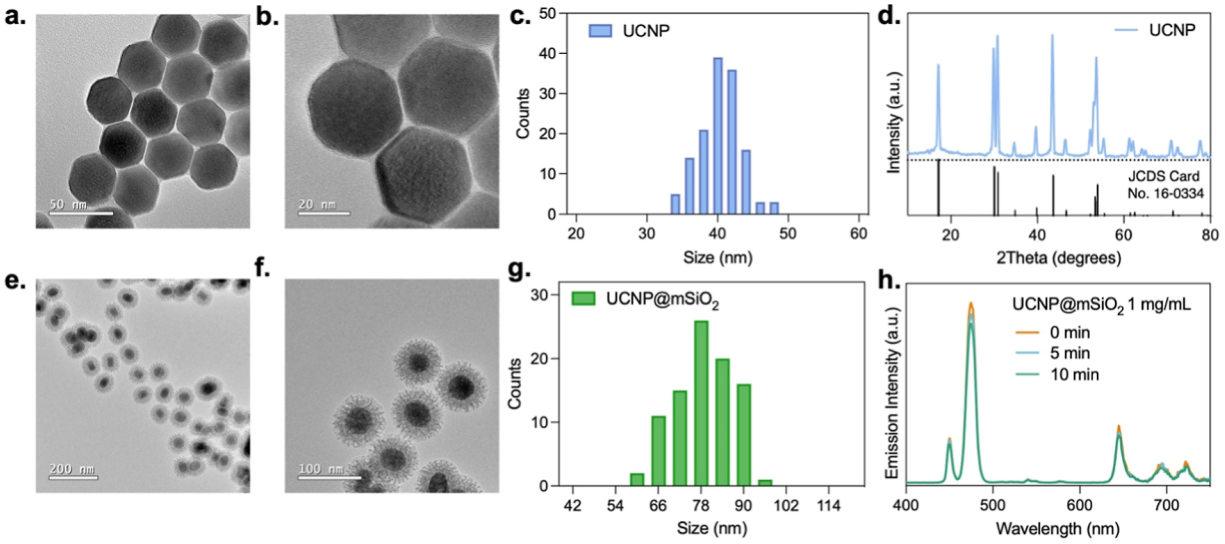

Figure 2. Nanoparticles characterization. (a,b) TEM images and (c) size distribution diagram of the UCNPs. The particles have approximately 40 nm. (d) XRD pattern of the prepared UCNPs and the reference pattern of the hexagonal (β) $NaYF_4$ (JCPDS, no. 16-0334). (e,f) TEM images and (g) size distribution diagram of UCNP@$mSiO_2$. The final particles have around 86 nm and the mesoporous silica shell have a thickness of 23 nm. (h) Emission spectra of UCNP@$mSiO_2$ aqueous solution (1 mg/mL) measured at three time points (0, 5, 10 min) showing the stability of the particles (λ_{exc} = 980 nm).

mL of CuCom dichloromethane solution with different concentrations (2, 4, and 10 mM = 10, 20, and 50 μmol). The system was kept under sonication for 1 h and then slowly allowed to dry overnight so the complex impregnated the silica shell.

Characterization. The size and shape of the UCNPs were studied with a FEI TECNAI20 transmission electron microscope. The powder's phase composition was determined by X-ray powder diffraction (XRD) using a Philips X'PERT (λ = 1.5406 Å). The luminescence emission spectra were recorded on a HORIBA Fluorolog TCSPC spectrofluorometer; for the upconversion, an external continuous 978 nm diode laser was used for excitation. The absorption spectra were measured using a PerkinElmer Lambda 1050 UV/vis/NIR spectrometer. Nitrogen adsorption/desorption analysis was measured using a Micromeritics ASAP 2020 M apparatus. The specific surface area was determined by the Brunauer−Emmett−Teller (BET) method. The pore volume was obtained from the T-plot method, and the average pore size was calculated using Barrett−Joiner−Halenda (BJH) method. The temperature-dependent spectral measurements were conducted using a Linkam temperature-controlled cooling and heating system (stage THMS600). Measurements of luminescence quenching, as a function of oxygen exposure, were performed using a controlled release of an O_2/N_2 (99.999%) mixture at a variable molar fraction of O_2 ranging from 0.0 to 1.0.

https://doi.org/10.1021/acsanm.4c06351
ACS Appl. Nano Mater. 2025, 8, 854−862

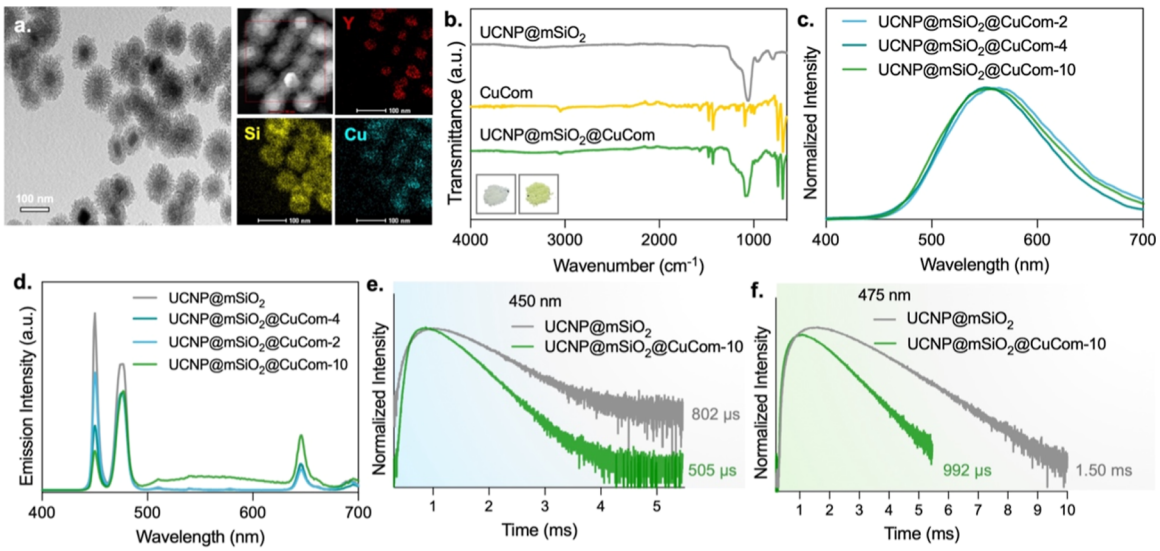

Figure 3. CuCom adsorption characterization. (a) TEM and EDS images of UCNPs@mSiO$_2$@CuCom-10. The colocalization of copper and silicon confirms the successful addition of CuCom to the mesoporous silica shell. (b) FTIR spectra of UCNPs@mSiO$_2$, CuCom, and UCNPs@mSiO$_2$@CuCom. The signals ascribed to the mesoporous silica shell and complex could be detected for UCNPs@mSiO$_2$@CuCom. (c) Emission spectra of UCNP@mSiO$_2$@CuCom-2, -4, and -10 (λ_{exc} = 360 nm). The emission is slightly blue-shifted for higher concentrations of CuCom due to the rigidochromic effect. (d) Emission spectra of UCNP@mSiO$_2$@CuCom-2, -4, and -10 (λ_{exc} = 980 nm) evidencing the decrease in the UCNPs emission in the UV-blue region and consequent appearance of the CuCom emission band in the red. The emission lifetime of UCNP@mSiO$_2$ and UCNP@mSiO$_2$@CuCom-10 measured at (e) 450 and (f) 475 nm. The shorter lifetime measured in the presence of CuCom indicates the occurrence of LRET.

RESULTS

Nanoplatform Working Principle. A schematic of the general working principle of the developed UCNP@mSiO$_2$@CuCom nanoplatform is shown in Figure 1a. To take advantage of the individual and combined properties of the materials, the Cu(I) complex was adsorbed to the UCNP@mSiO$_2$ surface and the energy transfer from the nanoparticles to the complex was explored. The CuCom structure and emissive properties were fully addressed in our previous work.[24] In summary, a butterfly shaped Cu_2I_2 core coordinates with triphenylphosphine and with a diphenyl-2-pyridyl-phosphine ligand (Figure 1b). The synthesized complex presents thermally activated delayed fluorescence emission (TADF), with maximums λ_{exc} = 320−370 nm and λ_{em} = 520−570 nm (Figure 1d). This property gives this type of complex highly efficient emission with a photoluminescent quantum yield close to 100%. Due to its low cost and high efficiency, this complex has been recognized as a promising material in the development of third-generation light-emitting devices.[25]

A schematic representation of the UCNP's energy levels is presented in Figure 1c. Upon excitation at 980 nm, Yb^{3+} acts as a well-known antenna, absorbing most of the excitation light and transferring it to the emitting Tm^{3+} ions. In the UCNPs emission spectrum shown in Figure 1d, it is possible to observe the characteristic emissions of Tm^{3+} in the UV, at 350 and 360 nm assigned to the $^1I_6 \rightarrow {}^3F_4$, and $^1D_2 \rightarrow {}^3H_6$ transitions, in the blue at 450 and 475 nm corresponding to the $^1D_2 \rightarrow {}^3F_4$ and $^1G_4 \rightarrow {}^3H_6$ transitions, and in the red, at 650 and 690 nm related to the $^1G_4 \rightarrow {}^3F_4$ and $^3F_3 \rightarrow {}^3H_6$ transitions. There is a strong overlap between the nanoparticles emission in the UV-blue regions and the complex absorption (Figure 1e), such that upon excitation of the UCNP@mSiO$_2$@CuCom at 980 nm, it was possible to detect an efficient energy transfer that leads to a decrease in the UCNP emission and consequent emergence of the CuCom luminescence. Based on these findings, we simultaneously explored the thermometric properties of the UCNPs, the oxygen sensing capabilities of the CuCom, and the color tuning potential attained by combining both materials.

Nanoplatform Synthesis and Characterization. *Up-converting Nanoparticles.* The $NaYF_4$:25% Yb^{3+},0.3Tm^{3+}@$NaYF_4$ UCNPs were synthesized through the high-temperature coprecipitation method. The produced particles have a size of approximately 40 nm, as determined by TEM (Figure 2a−c) and are highly crystalline with the pure hexagonal phase (JCPDS, no. 16-0334) of $NaYF_4$ crystal structure (Figure 2d). The core UCNPs were coated with a mesoporous silica shell using the two-phase method and the final UCNP@mSiO$_2$ structures have a diameter of approximately 86 nm with a silica shell thickness of about 23 nm (Figure 2e−g). The particle's surface area increased from 36 to 643 m^2/g after shell formation, and the pores have an approximate diameter of 2.5 nm (Figure S1). The mesoporous silica coating is known to decrease UCNP toxicity to biological systems,[26] and increase the nanoparticle's aqueous stability (Figure 2h) when compared to the as-prepared oleic acid-capped UCNP (UCNP@OA), which are hydrophobic and precipitate easily in aqueous media, as observable in the emission spectra shown in Figure S2. Additionally, the silica shell is transparent, presents oxygen permeability, and allows the addition of different CuCom concentrations through electrostatic interactions.

CuCom Adsorption. The UCNP@mSiO$_2$@CuCom were prepared by mixing the UCNPs@mSiO$_2$ with 2, 4, and 10 mM CuCom solutions (0.67, 1.33, and 2.5 μmol CuCom/g UCNP) and the produced samples were named UCNPs@mSiO$_2$@CuCom-2, UCNPs@mSiO$_2$@CuCom-4, and UCNPs@mSiO$_2$@CuCom-10, respectively. Based on energy-dispersive X-ray spectroscopy (EDS) mapping of sample UCNPs@mSiO$_2$@CuCom-10, shown in Figure 3a, the

https://doi.org/10.1021/acsanm.4c06351
ACS Appl. Nano Mater. 2025, 8, 854−862

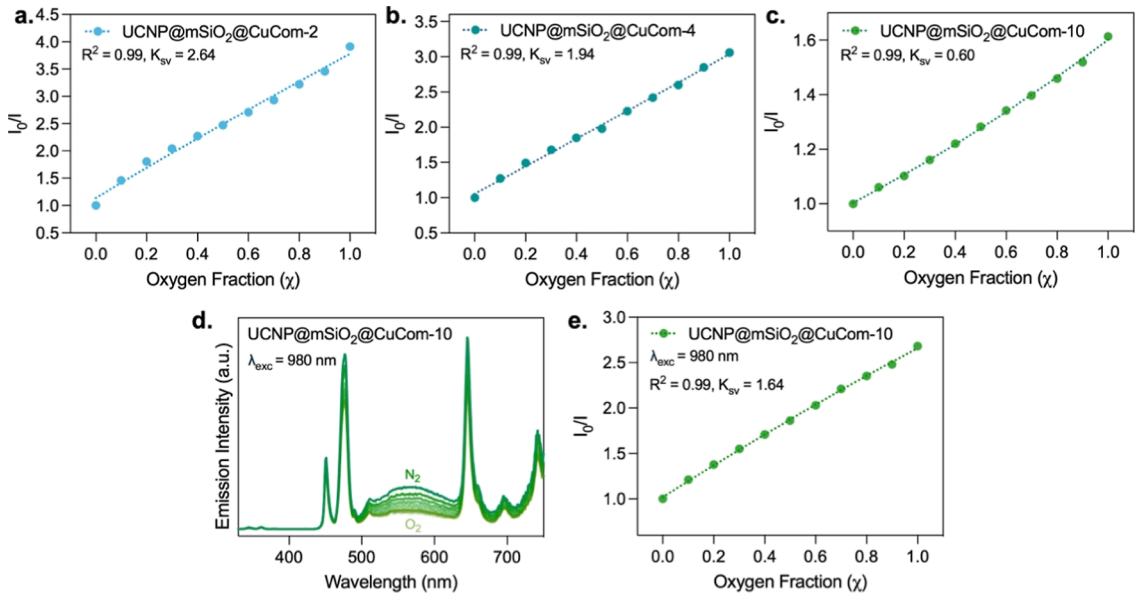

Figure 4. Oxygen sensing properties. The Stern−Volmer plots (I_0/I vs oxygen concentration) for (a) UCNP@$mSiO_2$@CuCom-2, (b) UCNP@$mSiO_2$@CuCom-4, and (c) UCNP@$mSiO_2$@CuCom-10 obtained upon excitation at 360 nm. The response to oxygen is higher for lower complex concentrations due to the lower degree of aggregation. (d) UCNP@$mSiO_2$@CuCom-10 emission spectra and (e) Stern−Volmer plot calculated for different oxygen fractions and under 980 nm excitation.

CuCom is uniformly distributed within the silica shell. We hypothesize that most molecules are electrostatically bound to the silica shell, however, chemical bonding may also occur, as suggested in other hybrid nanomaterials studies.[27] While this study focused on demonstrating the successful integration of CuCom into silica, further analysis would be necessary to define the exact nature of the interaction.

FTIR analysis also confirmed the successful addition of the complex (Figure 3b); corroborated by the clear changes in the nanoparticle's color from white to yellow (inset in Figure 3b). The UCNP@$mSiO_2$@CuCom-10 presented a combined FTIR spectrum of UCNP@$mSiO_2$ and CuCom, with silica absorption peaks at 1020−1110 cm^{-1} assigned to the Si−O−Si asymmetric stretching vibration, at 960 cm^{-1} ascribed to the asymmetric bending and stretching vibration of Si−OH, and the peaks associated with the complex at around 3050 cm^{-1} and below 1500 cm^{-1} due to the C−H and C−C stretching vibrations of the aromatic rings, respectively.

Upon excitation at 360 nm, only the CuCom luminescence was detected (Figure 3c), and the UCNPs@$mSiO_2$@CuCom-2 displayed a maximum emission at 560 nm, slightly shifted to longer wavelengths when compared to the nanoparticles containing 4 mM and 10 mM CuCom (λ_{em} = 550 nm). The shift is attributed to the rigidochromic effect and relates to molecular distortions upon the formation of the d−s excited state.[28,29] We hypothesize that part of the molecules entered the mesoporous silica shell pores, and, for the particles with a higher concentration of CuCom the complex became more aggregated on the silica surface having a lower degree of freedom for relaxation from the excited state.

To confirm the stability of CuCom within the silica matrix, we performed an emission-based washing experiment with UCNP@$mSiO_2$@CuCom-10. The nanomaterial was redispersed in water, kept under stirring for 20 min, and then centrifuged. Under excitation at 360 nm, the characteristic CuCom emission at 550 nm was observed for the UCNP@$mSiO_2$@CuCom-10, and the supernatant showed no detectable luminescent signal, indicating that the complex remained within the silica matrix without leaching (Figure S3). This result supports the stability of CuCom in our system, further confirming its effective integration within the mesoporous silica.

The particle's emission spectra upon 980 nm excitation are shown in Figure 3d. When compared to UCNP@$mSiO_2$, it was possible to detect clear decreases of 24%, 53%, and 59% in the UCNP's UV and blue emissions for UCNPs@$mSiO_2$@CuCom-2, UCNPs@$mSiO_2$@CuCom-4, and UCNPs@$mSiO_2$@CuCom-10, respectively. Despite the evidence of energy transfer in all samples, the molecule emission due to LRET was only detected for UCNPs@$mSiO_2$@CuCom-10, probably due to the requirement of higher complex concentration. A comparison of the excited state lifetime values of the emitting levels $^1D_2$ and $^1G_4$, measured for the emissions at 450 and 475 nm for the samples UCNP@$mSiO_2$ and UCNP@$mSiO_2$@CuCom-10, showed a decrease from 802 to 505 μs and from 1.50 ms to 992 μs, respectively, confirming the occurrence of efficient LRET in the latter (Figures 3e,f and S3 and S4).

Nanoplatform Properties. The energy coupling between the UCNPs and the complex made it possible to combine the properties of both materials to obtain synergistic systems capable of detecting molecular oxygen in downshifting and upconversion modes and performing thermometry. Additionally, varying the excitation wavelength and the temperature of the system enabled customized emission colors of the produced particles to attain additional functionality.

Oxygen Sensing. Sensing oxygen is crucial in many areas, from monitoring physiological functions in living organisms to controlling amounting and/or deficiency in various industrial and environmental applications. As previously demonstrated, combining CuCom with appropriate host matrices enables efficient O_2 sensing through luminescence quenching.[30,31] In the platform herein presented, the mesoporous silica shell allows gas permeation and provides good interaction between

https://doi.org/10.1021/acsanm.4c06351
ACS Appl. Nano Mater. 2025, 8, 854−862

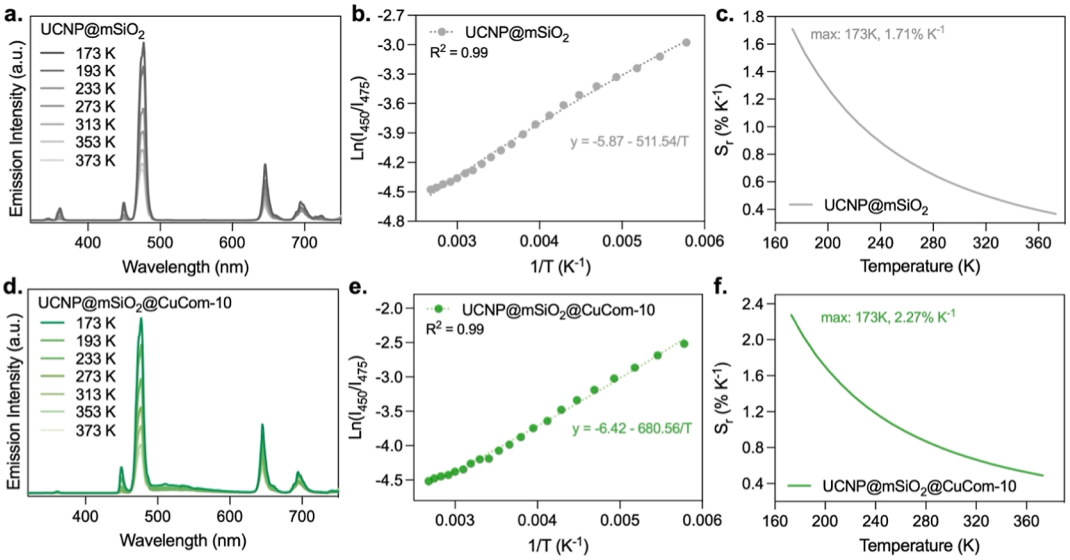

Figure 5. Optical thermometric properties in powder. Temperature-dependent emission spectra of (a) UCNP@mSiO$_2$ and (d) UCNP@mSiO$_2$@CuCom-10 (λ_{exc} = 980 nm). Ln(I_{450}/I_{475}) vs $1/T$ curves linearly fitted using the Boltzmann equation for (b) UCNP@mSiO$_2$ (R^2 = 0.9942) and (e) UCNP@mSiO$_2$@CuCom-10 (R^2 = 0.9948). The relative sensitivity evolution as a function of temperature for (c) UCNP@mSiO$_2$ and (f) UCNP@mSiO$_2$@CuCom-10. Higher sensitivity was achieved in the presence of CuCom probably due to the higher difference between the two analyzed emissions.

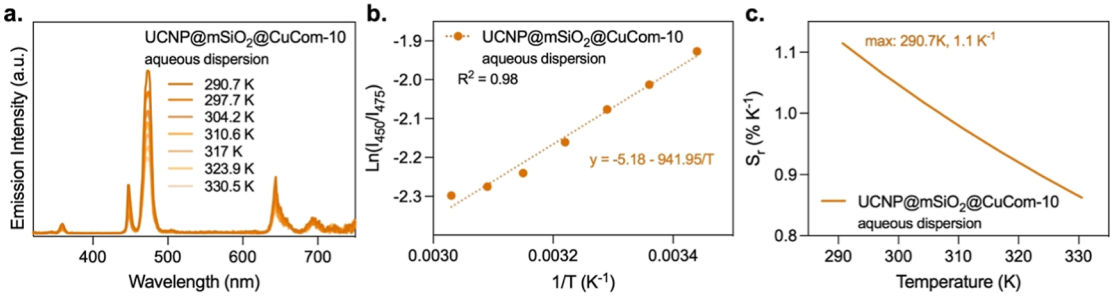

Figure 6. Optical thermometric properties of UCNP@mSiO$_2$@CuCom-10 in aqueous media. (a) Temperature-dependent emission spectra. (b) Ln(I_{450}/I_{475}) vs $1/T$ curves linearly fitted using the Boltzmann (R^2 = 0.9750). (c) The relative sensitivity evolution as a function of temperature.

the complex and oxygen molecules. In this way, our system can measure oxygen levels without chemically altering or directly interfering with the environment under analysis, allowing noninvasive sensing applications. The system's sensitivity was quantified by the Stern−Volmer constants (K_{sv}) obtained by fitting the I_0/I vs χ plots (where I = emission intensity and χ = oxygen fraction) and the obtained results are shown in Figure 4 (and Figure S4).

The Stern−Volmer plots obtained upon 360 nm excitation are presented in Figure 4a−c. The calculated K_{sv} values for UCNPs@mSiO$_2$@CuCom-2, -4, and -10 were 2.64, 1.94, and 0.60, respectively. The higher emission quenching and consequent higher sensitivity to O_2 obtained for the samples with lower concentrations of CuCom is due to the more evenly distributed molecules on the silica shell and lower degree of aggregation, which results in more effective interaction with the gas. This decrease in sensitivity was also observed for different Cu(I) complexes embedded in other mesoporous silica matrices.[19] In our previous work, the multifunctional platform based on a Cu(I) complex and UCNPs incorporated in a polystyrene matrix exhibited a response time to O_2 of approximately 5.5 s.[24] Based on it and on similar studies,[32,33] we anticipate comparable performance for the current system due to the similar structural and functional design, where the Cu(I) complex responds rapidly to oxygen.

The emission quenching caused by O_2 was also quantified by exploring the LRET mechanism (Figure 4d,e). Interestingly, when exciting the UCNPs@mSiO$_2$@CuCom-10 at 980 nm, the K_{sv} constant increased to 1.64, almost 3 times higher than the one obtained by direct complex excitation. Since the excitation comes from the nanoparticle core, this gain in sensitivity can be attributed to the excitation of the CuCom molecules, which are more evenly distributed inside the mesoporous silica pores. These results corroborate our previous hypothesis that part of the complex enters the pores and showcases the mesoporous silica shell's ability to function as an efficient matrix that allows oxygen permeation. In this way, using the developed nanoplatform, oxygen concentrations can be quantified at the nanoscale in both downshifting and upconversion modes, which gives high versatility and applicability to the system.

Thermometry. Optical nanothermometry is a powerful and versatile tool for remote temperature measurement at the nanoscale, with applications ranging from biomedical imaging to material science, and is continuously advancing with new technologies. In our system, the thermometric properties were explored using the luminescence intensity ratio between the

https://doi.org/10.1021/acsanm.4c06351
ACS Appl. Nano Mater. 2025, 8, 854−862

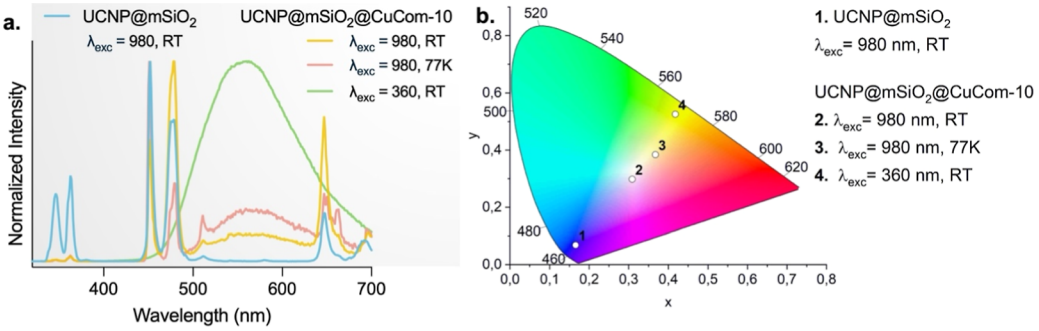

Figure 7. Color tuning properties. (a) Emission spectra and (b) CIE 1931 color space chromaticity diagram of UCNP@$mSiO_2$ and UCNP@$mSiO_2$@CuCom-10 under different excitation wavelengths and temperatures.

two nonthermally coupled Tm-UCNP emissions at 450 and 475 nm (I_{450}/I_{475}). We analyzed the thermometric response from 173 to 373 K for UCNP@$mSiO_2$ and UCNPs@$mSiO_2$@CuCom-10 in powder form, and the results are displayed in Figure 5. As expected, with temperature increase, the emission intensity decreases due to higher probability of nonradiative deactivation processes (Figure 5a,d). For both systems, the $\mathrm{Ln}(I_{450}/I_{475})$ vs $1/T$ curve resulted in a linear plot that could be fitted by the Boltzmann distribution eq (Figure 5b,e) in which $R_{ij} \propto \exp(\Delta E_{ij}/k_B T)$, where R_{ij} is the ratio between intensities at 450 and 475 nm, ΔE_{ij} is the energy difference between the emitting centers and k_B is the Boltzmann constant.

The relative sensitivity (S_r), defined by the equation: $S_r(T) = |R_{ij}^{-1}(dR_{ij}/dT)|$,[34] reached a maximum value of 1.71 and 2.27% K^{-1} at 173 K for UCNP@$mSiO_2$ and UCNPs@$mSiO_2$@CuCom-10, respectively. At room temperature (300 K), these values decreased to 0.6 and 0.9% K^{-1}, as shown in Figure 5c,f. We believe that the higher sensitivity achieved by the nanoplatform containing the complex is related to the occurrence of LRET, which resulted in a greater difference between the intensity of the analyzed emissions.

The thermometric response of UCNP@$mSiO_2$−CuCom-10 was also evaluated in an aqueous solution (1 mg/mL) across the temperature range of 290.7−330.5 K (Figure 6a) to assess its potential for biological applications. The $\mathrm{Ln}(I_{450}/I_{475})$ vs $1/T$ curve and calculated relative sensitivity are displayed in Figure 6b,c, and the results underscore the system's promise. The S_r maximum value reached 1.1% K^{-1} at 290.7 K and 1.0% K^{-1} at room temperature, which is higher than the value obtained for the powder sample.

Interestingly, the nanothermometric properties achieved with the combined UCNP and CuCom are superior to those using UCNPs alone, endorsing the use of the developed multifunctional material. This synergy between the materials can also be observed in the oxygen sensing measurement (K_{sv}) of the sample by exciting the complex indirectly at 980 nm on the UCNP@$mSiO_2$@CuCom-10 platform. Additionally, the performance of UCNP@$mSiO_2$−CuCom-10 in both powder and solution demonstrates its potential for use over a broad temperature range and under varying conditions while maintaining good sensitivity.

Color Tuning. The ability to tune colors at the nanoscale holds vast potential for advancing technology across various fields, from improving energy-efficient display technologies and biomedical imaging to enhancing security in counterfeiting. By adjusting the temperature and excitation wavelength, it was possible to modulate the emission of the produced particles. The resulting emission spectra are presented in Figure 7a and their corresponding points on the CIE 1931 color diagram are displayed in Figure 7b. At room temperature and under 980 nm excitation, UCNP@$mSiO_2$ emitted primarily blue light at around 460 nm, with x, y coordinates of 0.16, 0.068. However, for UCNP@$mSiO_2$@CuCom-10 under the same conditions, an almost white color was achieved, with x, y coordinates of 0.30, 0.30. When the temperature is decreased to 77 K while maintaining the excitation, the color shifts to a yellowish tone, with x, y coordinates of 0.37, 0.38. Additionally, direct excitation of the complex at 360 nm results in an emission at 570 nm, with x, y coordinates of 0.42, 0.52.

This modulation capability allows the system to achieve a broad range of colors, including blue, white, and yellow tones. The color-tuning property achieved by combining UCNPs with CuCom enhances the versatility of our nanoplatform, enabling precise control and customized emission for various applications, such as bioimaging and advanced display technologies.

The combination of properties in our platform offers significant advantages in application scenarios requiring multiparametric monitoring. For example, ensuring appropriate oxygen levels and temperature is critical for cell viability in tissue engineering and cell culture. Our nanosystem can provide real-time feedback for optimized growth conditions. Moreover, it can provide enhanced control over oxygen sensing and temperature monitoring in catalytic processes, which are indispensable for controlling reaction environments and improving catalytic efficiency. In environmental monitoring, fluctuations in oxygen concentration and temperature often occur simultaneously. For instance, in water quality monitoring, oxygen levels and temperature changes can indicate pollution or eutrophication. By combining these functionalities in a single platform, we provide a powerful tool for multiparametric sensing in these and other fields, enhancing the precision and versatility of the sensing technology. Moreover, the added emission color tuning allows for multiplexing, where different emission colors could represent different analytes or environmental parameters.

CONCLUSION

In conclusion, we have successfully developed and demonstrated a multifunctional nanoplatform by integrating an upconversion nanoparticle (Tm-UCNPs@$mSiO_2$) with a Cu(I) emissive complex (CuCom) within the mesoporous silica shell of the core particle. This innovative system leverages the unique properties of both components, resulting in a highly versatile material capable of noninvasive oxygen sensing, optical thermometry, and emission color tuning. We explored

https://doi.org/10.1021/acsanm.4c06351
ACS Appl. Nano Mater. 2025, 8, 854−862

the LRET mechanism between the UCNPs and CuCom, which significantly enhanced the platform's functionality, enabling efficient CuCom red emission and sensitive response to molecular oxygen in upconversion mode. Our detailed characterization and testing revealed that the optimized UCNP@mSiO$_2$@CuCom-10 platform performs remarkably in various applications. The platform's high sensitivity to oxygen makes it suitable for environmental monitoring, industrial safety, and biological studies, where accurate and sensitive measurements of oxygen levels are critical. Additionally, its precise optical thermometric capabilities, with relative sensitivities of up to 2.27% K^{-1} at 173 K, highlight its potential for use in biomedical imaging and material science, providing noninvasive and real-time temperature measurements. Furthermore, the emission color tuning property of the nanoplatform, achieved by varying the excitation wavelength and temperature, adds another layer of functionality, making it applicable in advanced display technologies and bioimaging. The ability to modulate emission colors from blue to white and yellow enhances its versatility, paving the way for customized solutions in various technological and scientific fields. Overall, the UCNP@mSiO$_2$@CuCom system represents an advancement in the development of multifunctional nanomaterials. Its smart design, combined with excellent luminescent properties, positions it as a promising candidate for various applications, including those based on the next (third) generation of light-emitting devices. The successful synthesis and comprehensive evaluation of this nanoplatform underscore its potential to drive innovation and address complex challenges across multiple disciplines.

■ ASSOCIATED CONTENT

Supporting Information

The Supporting Information is available free of charge at https://pubs.acs.org/doi/10.1021/acsanm.4c06351.

Additional characterization of the materials and nanoplatforms. It covers surface area and pore size measurements, stability tests of UCNP-based solutions, elemental analysis via EDS mapping, and washing experiments to confirm the retention of complexes within silica matrices. Emission spectra are provided to demonstrate the upconversion properties, including the effect of laser power on emission and the associated lifetimes. Additionally, oxygen sensing performance across different nanoplatforms is also presented (PDF)

■ AUTHOR INFORMATION

Corresponding Authors

Marylyn Setsuko Arai − *São Carlos Institute of Physics, University of São Paulo, 13566-590 São Carlos, Brazil;* orcid.org/0000-0003-1278-5274; Email: marylyn.setsuko@gmail.com

Andrea Simone Stucchi de Camargo − *Federal Institute for Materials Research and Testing (BAM), 12489 Berlin, Germany; Otto-Schott Institute of Materials Research, Friedrich-Schiller University (FSU), 07743 Jena, Germany;* orcid.org/0000-0001-8352-2573; Email: andrea.camargo@bam.de

Authors

Leandro Piaggi Ravaro − *São Carlos Institute of Physics, University of São Paulo, 13566-590 São Carlos, Brazil;*

Mariana Amorim Sigoli − *São Carlos Institute of Physics, University of São Paulo, 13566-590 São Carlos, Brazil;*

Gustavo Vinicius Bassi − *Graduate Program on Physics Engineering, Federal Rural University of Pernambuco, 54518-430 Cabo de Santo Agostinho, Brazil*

Gabriel Brambilla − *São Carlos Institute of Physics, University of São Paulo, 13566-590 São Carlos, Brazil;* orcid.org/0000-0003-1382-866X

Lauro June Queiroz Maia − *Physics Institute, Federal University of Goiás, 74690-900 Goiânia, Brazil*

Mohammad Reza Dousti − *Graduate Program on Physics Engineering, Federal Rural University of Pernambuco, 54518-430 Cabo de Santo Agostinho, Brazil*

Complete contact information is available at: https://pubs.acs.org/10.1021/acsanm.4c06351

Author Contributions

#M.S.A. and L.P.R. contributed equally to this paper.

Funding

The Article Processing Charge for the publication of this research was funded by the Coordination for the Improvement of Higher Education Personnel - CAPES (ROR identifier: 00x0ma614).

Notes

The authors declare no competing financial interest.

■ ACKNOWLEDGMENTS

The authors acknowledge the financial support from the funding agencies CAPES—Coordenação de Aperfeiçoamento de Pessoal de Nível Superior (Finance code 001), CNPq—Conselho Nacional de Desenvolvimento Científico e Tecnológico, FAPESP—Fundação de Amparo à Pesquisa do Estado de São Paulo (grant no. 2021/01170-3, and Cepid Project no. 2013/07793-6 and FAPEG—Fundação de Amparo à Pesquisa do Estado de Goiás; CeRTEV—Center for Research Technology and Education on Vitreous Materials) and CEHTES—Centro de Excelência em Hidrogênio e Tecnologias Energéticas Sustentáveis. M.S.A. acknowledges FAPESP for granting the doctoral fellowship (grant no. 2019/12588-9). LPR is additionally thankful to FACEPE—Pernambuco Science Foundation, for the grants APQ-0096-3.03/19 and DCR-0010-3.03/21. G.V.B. acknowledges CAPES for granting the master's fellowship (Process no. 88887.666855/2022-00).

■ REFERENCES

(1) Suh, W. H.; Suh, Y.-H.; Stucky, G. D. Multifunctional Nanosystems at the Interface of Physical and Life Sciences. *Nano Today* **2009**, *4* (1), 27−36.

(2) *Nanomaterials*; Edelstein, A. S., Cammaratra, R. C., Eds.; CRC Press, 1998.

(3) Roduner, E. Size Matters: Why Nanomaterials Are Different. *Chem. Soc. Rev.* **2006**, *35* (7), 583.

(4) Haase, M.; Schäfer, H. Upconverting Nanoparticles. *Angew. Chem., Int. Ed.* **2011**, *50* (26), 5808−5829.

(5) Wilhelm, S. Perspectives for Upconverting Nanoparticles. *ACS Nano* **2017**, *11* (11), 10644−10653.

(6) Arai, M. S.; de Camargo, A. S. S. Exploring the Use of Upconversion Nanoparticles in Chemical and Biological Sensors: From Surface Modifications to Point-of-Care Devices. *Nanoscale Adv.* **2021**, *3*, 5135.

(7) Grüner, M. C.; Arai, M. S.; Carreira, M.; Inada, N.; de Camargo, A. S. S. Functionalizing the Mesoporous Silica Shell of Upconversion Nanoparticles To Enhance Bacterial Targeting and Killing via Photosensitizer-Induced Antimicrobial Photodynamic Therapy. *ACS Appl. Bio Mater.* **2018**, *1* (4), 1028−1036.

(8) Arai, M. S.; Kim, H.; Pascavis, M.; Cha, B.; Brambilla, G.; Cho, Y. K.; Park, J.; Vilela, R. R. C.; de Camargo, A. S. S.; Castro, C. M.; Lee, H. Upconverting Nanoparticle-Based Enhanced Luminescence Lateral-Flow Assay for Urinary Biomarker Monitoring. *ACS Appl. Mater. Interfaces* **2024**, *16* (29), 38243−38251.
(9) Wang, C.; Jin, Y.; Zhang, R.; Yao, Q.; Hu, Y. A Review and Outlook of Ratiometric Optical Thermometer Based on Thermally Coupled Levels and Non-Thermally Coupled Levels. *J. Alloys Compd.* **2022**, *894*, 162494.
(10) He, L.; Huang, J.; An, Z.; Huang, H.; Zhao, Y.; Zhong, K.; Zhou, B. Achieving Thermochromic Upconversion of Tm3+ for High-Sensitive Nanoprobe and Information Encryption. *J. Lumin.* **2024**, *266*, 120306.
(11) Zink, D. M.; Volz, D.; Baumann, T.; Mydlak, M.; Flügge, H.; Friedrichs, J.; Nieger, M.; Bräse, S. Heteroleptic, Dinuclear Copper(I) Complexes for Application in Organic Light-Emitting Diodes. *Chem. Mater.* **2013**, *25* (22), 4471−4486.
(12) Li, S.; Cao, D.; Meng, X.; Hu, Z.; Li, Z.; Yuan, C.; Zhou, T.; Han, X.; Ma, W. A Novel Fluorescent Sensor for Specific Recognition of GSH Based on the Copper Complex and Its Bioimaging in Living Cells. *Bioorg. Chem.* **2020**, *100*, 103923.
(13) Kalinichev, A. A.; Shamsieva, A. V.; Strelnik, I. D.; Musina, E. I.; Lähderanta, E.; Karasik, A. A.; Sinyashin, O. G.; Kolesnikov, I. E. Binuclear Charged Copper(I) Complex as a Multimode Luminescence Thermal Sensor. *Sens. Actuators, A* **2021**, *325*, 112722.
(14) Cariati, E.; Bu, X.; Ford, P. C. Solvent- and Vapor-Induced Isomerization between the Luminescent Solids $[CuI(4\text{-}Pic)]_4$ and $[CuI(4\text{-}Pic)]_\infty$ (Pic = Methylpyridine). The Structural Basis for the Observed Luminescence Vapochromism. *Chem. Mater.* **2000**, *12* (11), 3385−3391.
(15) Smith, C. S.; Branham, C. W.; Marquardt, B. J.; Mann, K. R. Oxygen Gas Sensing by Luminescence Quenching in Crystals of $Cu(Xantphos)(Phen)^+$ Complexes. *J. Am. Chem. Soc.* **2010**, *132* (40), 14079−14085.
(16) Zhang, L.; Lin, F.; Ye, M.; Tian, D.; Jin, J.; Huang, Y.; Jiang, Y.; Wang, Y.; Chen, X. Luminescence Sensing of Oxygen Using Copper Iodide Hybrid Material. *Sens. Actuators, B* **2021**, *346*, 130566.
(17) Dias, H. V. R.; Diyabalanage, H. V. K.; Rawashdeh-Omary, M. A.; Franzman, M. A.; Omary, M. A. Bright Phosphorescence of a Trinuclear Copper(I) Complex: Luminescence Thermochromism, Solvatochromism, and "Concentration Luminochromism. *J. Am. Chem. Soc.* **2003**, *125* (40), 12072−12073.
(18) Ohara, H.; Ogawa, T.; Yoshida, M.; Kobayashi, A.; Kato, M. Reversible Luminescent Colour Changes of Mononuclear Copper(I) Complexes Based on Ligand Exchange Reactions by N-Heteroaromatic Vapours. *Dalton Trans.* **2017**, *46* (11), 3755−3760.
(19) Ravaro, L. P.; Almeida, T. R.; Albuquerque, R. Q.; de Camargo, A. S. S. The Polynuclear Complex $Cu_4I_4Py_4$ Loaded in Mesoporous Silica: Photophysics, Theoretical Investigation, and Highly Sensitive Oxygen Sensing Application. *Dalton Trans.* **2016**, *45* (44), 17652−17661.
(20) Ravaro, L. P.; Mafud, A. C.; Li, Z.; Reinheimer, E.; Simone, C. A.; Mascarenhas, Y. P.; Ford, P. C.; de Camargo, A. S. S. New Emissive Mononuclear Copper (I) Complex: Structural and Photophysical Characterization Focusing on Solvatochromism, Rigidochromism and Oxygen Sensing in Mesoporous Solid Matrix. *Dyes Pigm.* **2018**, *159*, 464−470.
(21) Ramamoorthy, R.; Dutta, P. K.; Akbar, S. A. Oxygen Sensors: Materials, Methods, Designs and Applications. *J. Mater. Sci.* **2003**, *38* (21), 4271−4282.
(22) Wang, X.; Wolfbeis, O. S. Optical Methods for Sensing and Imaging Oxygen: Materials, Spectroscopies and Applications. *Chem. Soc. Rev.* **2014**, *43* (10), 3666−3761.
(23) Papkovsky, D. B. New Oxygen Sensors and Their Application to Biosensing. *Sens. Actuators, B* **1995**, *29* (1−3), 213−218.
(24) Ravaro, L. P.; Arai, M. S.; Maia, L. J. Q.; Reza Dousti, M.; Santiago, P. H. de O.; Ellena, J.; de Camargo, A. S. S. Multifunctional Platform Based on a Copper(I) Complex and $NaYF_4$:Tm^{3+}, Yb^{3+} Upconverting Nanoparticles Immobilized into a Polystyrene Matrix: Downshifting and Upconversion Oxygen Sensing. *ACS Appl. Mater. Interfaces* **2022**, *14* (42), 47902−47912.
(25) Wallesch, M.; Volz, D.; Zink, D. M.; Schepers, U.; Nieger, M.; Baumann, T.; Bräse, S. Bright Coppertunities: Multinuclear Cu^I Complexes with N−P Ligands and Their Applications. *Chem. - Eur. J.* **2014**, *20* (22), 6578−6590.
(26) Zhou, M.; Ge, X.; Ke, D.-M.; Tang, H.; Zhang, J.-Z.; Calvaresi, M.; Gao, B.; Sun, L.; Su, Q.; Wang, H. The Bioavailability, Biodistribution, and Toxic Effects of Silica-Coated Upconversion Nanoparticles in Vivo. *Front Chem.* **2019**, *7*, 218.
(27) Sanchez, C.; Belleville, P.; Popall, M.; Nicole, L. Applications of Advanced Hybrid Organic−Inorganic Nanomaterials: From Laboratory to Market. *Chem. Soc. Rev.* **2011**, *40* (2), 696.
(28) Kondo, S.; Yoshimura, N.; Yoshida, M.; Kobayashi, A.; Kato, M. Vapochromic Luminescence of a Spin-Coated Copper(I) Complex Thin Film by the Direct Coordination of Vapour Molecules. *Dalton Trans.* **2020**, *49* (46), 16946−16953.
(29) Watts, R. J.; Missimer, D. Environmentally Hindered Radiationless Transitions between States of Different Orbital Parentage in Iridium(III) Complexes. Application of Rigid-Matrix Induced Perturbations of the Pseudo-Jahn-Teller Potential to the Rigidochromic Effect in D6Metal Complexes. *J. Am. Chem. Soc.* **1978**, *100* (17), 5350−5357.
(30) Medina-Rodríguez, S.; Orriach-Fernández, F. J.; Poole, C.; Kumar, P.; de la Torre-Vega, A.; Fernández-Sánchez, J. F.; Baranoff, E.; Fernández-Gutiérrez, A. Copper(I) Complexes as Alternatives to Iridium(III) Complexes for Highly Efficient Oxygen Sensing. *Chem. Commun.* **2015**, *51* (57), 11401−11404.
(31) Hui, H.; Wei, L.; Zhentao, L.; Xiangen, H. A Green-Emitting Cu Complex for Oxygen-Sensing Purpose: Synthesis, Characterization and Photophysical Features. *Spectrochim. Acta, Part A* **2015**, *142*, 271−278.
(32) Smith, C. S.; Mann, K. R. Exceptionally Long-Lived Luminescence from $[Cu(I)(Isocyanide)_2(Phen)]^+$ Complexes in Nanoporous Crystals Enables Remarkable Oxygen Gas Sensing. *J. Am. Chem. Soc.* **2012**, *134* (21), 8786−8789.
(33) Wang, Y.; Li, B.; Liu, Y.; Zhang, L.; Zuo, Q.; Shi, L.; Su, Z. Highly Sensitive Oxygen Sensors Based on Cu(i) Complex−Polystyrene Composite Nanofibrous Membranes Prepared by Electrospinning. *Chem. Commun.* **2009**, *39*, 5868.
(34) Silva, A. F.; Elan, F.; Falcão-Filho, E. L.; Maia, L. J. Q.; de Araújo, C. B. Thermal Sensitivity of Frequency Upconversion in $Al_4B_2O_9$:Yb^{3+}/Nd^{3+} Nanoparticles. *J. Mater. Chem. C* **2017**, *5* (5), 1240−1246.
(35) Gnanasammandhan, M. K.; Idris, N. M.; Bansal, A.; Huang, K.; Zhang, Y. Near-IR Photoactivation Using Mesoporous Silica-Coated $NaYF_4$:Yb,Er/Tm Upconversion Nanoparticles. *Nat. Protoc.* **2016**, *11* (4), 688−713.
(36) Cichos, J.; Karbowiak, M. A General and Versatile Procedure for Coating of Hydrophobic Nanocrystals with a Thin Silica Layer Enabling Facile Biofunctionalization and Dye Incorporation. *J. Mater. Chem. B* **2014**, *2* (5), 556−568.
(37) Volz, D.; Zink, D. M.; Bocksrocker, T.; Friedrichs, J.; Nieger, M.; Baumann, T.; Lemmer, U.; Bräse, S. Molecular Construction Kit for Tuning Solubility, Stability and Luminescence Properties: Heteroleptic MePyrPHOS-Copper Iodide-Complexes and Their Application in Organic Light-Emitting Diodes. *Chem. Mater.* **2013**, *25* (17), 3414−3426.

https://doi.org/10.1021/acsanm.4c06351
ACS Appl. Nano Mater. 2025, 8, 854−862